frontiers in Earth Science

ORIGINAL RESEARCH
published: 07 March 2022
doi: 10.3389/feart.2022.851236

Effect of Terrigenous Sediment Addition on the Generation of Arc Silicic Magma: Constraints From the Comparative Partial Melting Experiment at 1.5 GPa

Chunjuan Zang[1,2,3] *and Mingliang Wang*[1,2,3]*

[1]School of Resource and Civil Engineering, Suzhou University, Suzhou, China, [2]National Engineering Research Centre of Coal Mine Water Hazard Controlling, Suzhou, China, [3]Key Laboratory of Mine Water Resource Utilization of Anhui Higher Education Institutes, Suzhou University, Suzhou, China

To assess the effects of sediment addition on the partial melting of subducted oceanic crust and generation of arc silicic magma, a series of comparative partial melting experiments on a garnet plagioamphibolite and a 90 wt% garnet plagioamphibolite + 10 wt% plagioclase slate mixture at 850–1,000°C/1.5 GPa were conducted on a Piston-cylinder apparatus. In the experimental products, partial melt coexists with amphibole + plagioclase + garnet + clinopyroxene at 850–950°C and plagioclase + garnet + clinopyroxene at 1000°C. Compared with pure garnet plagioamphibolite, partial melting of mixture get a higher melting percentage and generates the silicic melt with geochemical characteristics of higher Na_2O/K_2O and lower Al_2O_3 in major element and high Rb content in trace element at over 950°C. This result indicates that silicic arc magma may generate from partial melting of metamorphic subducted oceanic crust with sediments thereon, sediment addition contributes to their chemical component and generation dynamic process.

Keywords: arc silicic magma, partial melting, subducted oceanic crust, sediment, experimental petrology

OPEN ACCESS

Edited by:
Lidong Dai,
Institute of geochemistry (CAS), China

Reviewed by:
Sheqiang Miao,
China Earthquake Administration, China
Dawei Fan,
Institute of Geochemistry (CAS), China

***Correspondence:**
Mingliang Wang
wangapple1999@126.com

Specialty section:
This article was submitted to Petrology, a section of the journal Frontiers in Earth Science

Received: *09 January 2022*
Accepted: *26 January 2022*
Published: *07 March 2022*

Citation:
Zang C and Wang M (2022) Effect of Terrigenous Sediment Addition on the Generation of Arc Silicic Magma: Constraints From the Comparative Partial Melting Experiment at 1.5 GPa. Front. Earth Sci. 10:851236. doi: 10.3389/feart.2022.851236

INTRODUCTION

According to plate tectonics, convergent plate margins are the most active areas on earth. The oceanic plate is dehydrated during subduction at these margins. During this subduction, the oceanic plate releases fluids, and these fluids join the overlying mantle wedge, causing partial melting of the mantle wedge and generating island arc basaltic magma (Sun et al., 2014; Zheng et al., 2015; Li and Ni, 2020; Liu et al., 2019; Zheng et al., 2019; Wei and Zheng, 2020; Xiong et al., 2020). Besides the basalt, there are a number of silicic magmas located on convergent plate margins (even typical oceanic island arcs, such as Tonga and the Kuril Islands), as shown in **Figure 1**. These magmas cannot be formed by partial melting of the peridotite mantle wedge, even ~52 wt% SiO_2 melt could be generated by a very low degree (~2 wt%) partial melt of peridotite in the upper mantle wedge (Baker et al., 1995), but such a low percentage partial melting cannot generate real magma due to magmatic dynamic characteristics. While the melting percentage increases, the SiO_2 content of melts from partial melting of peridotite will decrease rapidly, so partial melting of the mantle cannot generate silicic magma generally.

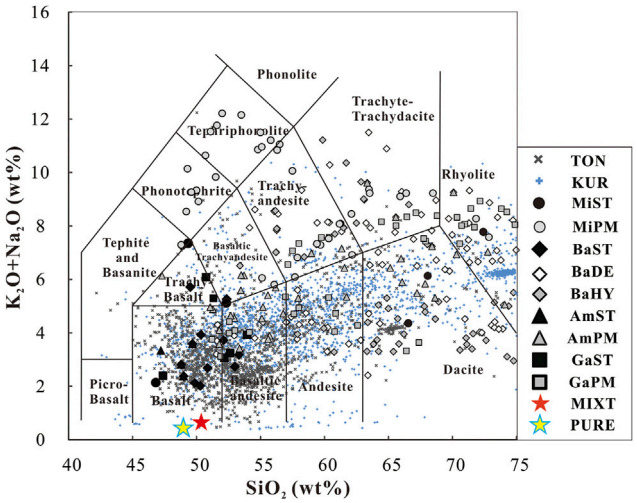

FIGURE 1 | Total alkali versus silica (TAS) variation diagram of basic rocks and their product-melts in partial melting experiments. This figure is modified from **Figure 2** in Zang et al. (2020), Classification and nomenclature of TAS diagram follow Maitre (1989). BaST, starting material of basalts; BaDE, melts generate in basalts' partial melting experiments; BaHY, melts generate in partial melting of hydrous basalt (Beard and Lofgren 1991; Qian and Hermann 2013; Rapp and Watson 1995; Rapp, et al., 1991; Rushmer 1991; Sisson, et al., 2005; Takahahshi, et al., 1998; Xiong, et al., 2005, 2006; Yaxley and Green 1998). AmST, starting material of amphibolites; AmPM, melts generated in partial melting experiments on amphibolites (Sen and Dunn 1994; Rapp and Watson 1995). GaST, starting material of gabbros; GaPM, melts generate in partial melting experiments on gabbros (Koepke, et al., 2004; Sisson,et al., 2005). MiST, starting material of mixtures (basalt + sediment or mélange); MiPM, melts from partial melting experiments on these mixtures (Cruz-Uribe et al., 2018; Zang et al., 2020). PURE, pure starting material used in this paper, 18TH-02 (garnet plagioamphibolite, as a representative of metamorphic oceanic crust), MIXT, mixture starting material used in this paper, 90wt% 18TH-02 + 10wt% 18 TH-07 (plagioclase slate, as a representative of metamorphic terrigenous sediment), TON, magmatic rocks located at Tonga island arc; KUR, magmatic rocks located at the Kuril Islands, data on TON and KUR are from the GEOROC web site (http://georoc.mpch-mainz.gwdg.de/georoc/).

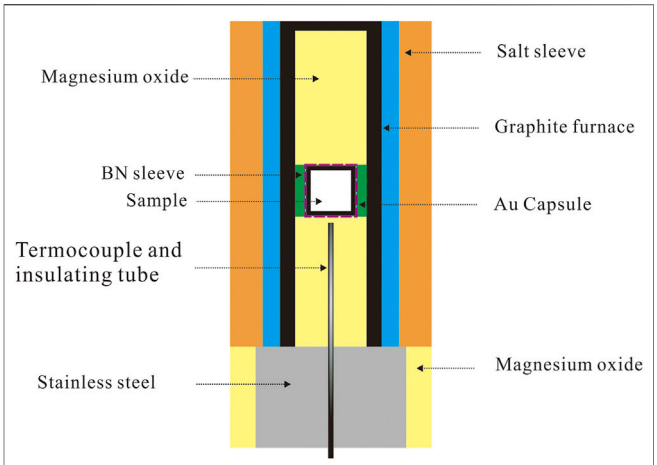

FIGURE 2 | Sketch map of sample assemblage.

The magmas on oceanic islands that arc without a continental crust (such as Tonga) are not generated by hybridized basaltic magma by crust or the partial melting of continental lower crust *via* the heating process. These silicic magmas could then generate from: 1) fractionation of basaltic or andesitic parents magma (Nandedkar et al., 2014; Peter et al., 2018); 2) partial melting of subducted sediments (Tatsumi, 2001); 3) partial melting of subducted basaltic oceanic crust with or without sediments. For the 1) fractionation model, the sticky silicic magmas need to separate from amphibole (Amp) ± clinopyroxene (Cpx) ± orthopyroxene (Opx) utterly, avoiding the reduction of their whole rock SiO_2 content. This dynamic process makes the fractionation model unacceptable. For the 2) partial melting of sediments individually, there are also some insoluble problems. These oceanic sediments could partially melt individually (Tatsumi, 2001; Hermann and Spandler, 2008; Hu et al., 2017; Frster and Selway, 2021), but the characteristic of major-trace element and isotope for the overwhelming majority of arc magma needs oceanic crust in their magmatic source (Hildreth and Moorbath, 1988; Elliott, 2003; Cruz-Uribe et al., 2018; Wang et al., 2021). This indicates that the silicic magmas could only generate *via* partial melting of subducted basaltic oceanic crust with or without sediments. For the same reasons as those oputlined in hypothesis 2), these silicic magmas need sediments in their magmatic source, and the sediments in arc could detect the magmatic source *via* characteristics of trace elements and isotopes (Tera et al., 1986; Hildreth and Moorbath, 1988; Morris et al., 1990; Plank, 2005; Hu et al., 2017; Nielsen and Marschall, 2017; Shu et al., 2017; Cruz-Uribe et al., 2018; Zang et al., 2020). How these sediments effect magma generation during mixture cases is a key question that it is difficult to answer *via* field observation. The studies mentioned above (Tera et al., 1986; Morris et al., 1990; Hu et al., 2017; Nielsen and Marschall, 2017; Shu et al., 2017) could not only reveal the existence of sediments at magmatic source, but not their affect. The only way to solve this problem is by conducting high temperature and high pressure partial melting experiments, comparing the difference in partial melting behavior between pure basic rocks and basalt-sediments mixture.

A number of previous studies have focussed on the partial melting of basic rocks (Beard and Lofgren, 1991; Rapp et al., 1991; Rushmer, 1991; Sen and Dunn, 1994; Rapp and Watson, 1995; Takahahshi et al., 1998; Yaxley and Green, 1998; Koepke et al., 2004; Sisson et al., 2005; Xiong et al., 2005; Xiong et al., 2006; Qian and Hermann, 2013). These findings have revealed the partial melting behavior of pure basaltic oceanic crust during the subduction process; however, studies focussing on the partial melting of basic rock and sediment are very limited (Mccarthy and Patiño Douce, 1997; Zang et al., 2020). The studies that have been conducted show that even a small amount of sediment addition in basalt could effect the partial melting behavior, which is noteworthy. The effects include: 1) that sediment addition enhanced the partial melting ratio of basalt, as confirmed by similar studies (Zhang et al., 2019; Zhang Y. et al., 2020; Pelleter et al., 2021); 2) sediment addition changed the chemical component of the partial melts generated in these experiments, compared with the one from pure basalt.

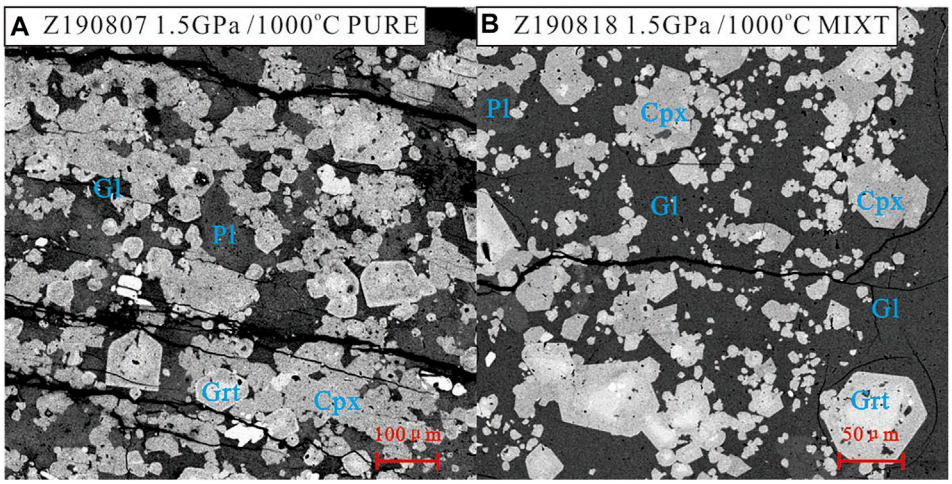

FIGURE 3 | Representative BSE photos of experiment products. Phase abbreviation: Gl = glass (melt), Cpx = clinopyxene, Grt = garnet, Pl = plagioclase.

According to existing research, we could get an outline of the effect caused by the addition of sediments during the partial melting of subducted basaltic oceanic crust; however, there are some important questions remaining, including: 1) that sediment addition could enhance the partial melting ratio, but in what conditions? How much is the increase of ratio; 2) what is the composition difference between melts from pure basalt and mixture of basalt-sediment? These two questions are very important for understanding the effect of sediment addition in basalt and the generation of silicic magmas located on convergent plate margins. In order to understand the effect of the partial melting of the subducted basaltic oceanic crust, caused by the addition of a small amount terrigenous sediment, a series of comparative partial melting experiments were conducted on a garnet plagioamphibolite and a 90 wt% garnet plagioamphibolite + 10 wt% plagioclase slate at 850–1,000°C/1.5 GPa in this study. In the following sections, we will describe the starting materials and analytical methods, firstly, and then comparing partial melts from pure and mixture. At last, we will highlight a natural example of rocks from Tonga and Kuril, which verifies the strong effects of the addition of a small amount of sediment during the partial melting of subducted oceanic basalt at convergent plate margins.

EXPERIMENTAL AND ANALYTICAL METHODS

Starting Materials

During the subduction process, the basaltic oceanic crust may become garnet plagioamphibolite while the terrigenous sediments (mud) may transform into slate at 1.5–2.0 GPa. As the oceanic crust could then partially melt at high geothermal gradient (at approximately 1.5–2.0 GPa and ~900°C), we chose 1.5 GPa and 850–1,000°C as run conditions in this study (Zheng et al., 2015; Wei and Zheng, 2020; Zhang Z. et al., 2020).

Two metamorphic rocks were chosen to prepare the starting materials. The 18TH-02 is a garnet plagioamphibolite and contains 50 vol% Amp, 35 vol% plagioclase (Pl), 12 vol% garnet (Grt), and trace amounts of V-Ti magnetite. Its major element composition is very similar to the average composition of oceanic crust, and several important trace elements (such as V, Cr, Rb, and Sr) of 18TH-02 are also close to the average composition of oceanic crust. The terrigenous sediment is represented by a plagioclase slate (18TH-07), this sample contains 85 vol% feldspar (orthoclase + albite + plagioclase), 10 vol% mica, and trace amounts of quartz. Their major element composition and selected trace elements are very close to the Upper Continental Crust (UCC) (the data of these two metamorphic rocks is listed in **Supplementary Table S1**).

Both of these rocks were collected from Susong, Anhui Province, China. The two rocks (18TH-02 and 18TH-07) were ultrasonically cleaned in distilled water and alcohol successively, and then crushed to powder to ~120 meshes separately. In order to simulate the partial melting process of the oceanic crust with or without terrigenous sediments thereon during subduction process, two starting materials were used: PURE and MIXT. The PURE is representative of pure basaltic oceanic crust, which was made by 18TH-02 power only. The MIXT is representative of basaltic oceanic crust with terrigenous sediment, which was made by mixture 90 wt% 18TH-02 power and 10 wt% 18TH-07 power. The proportion was determine by typical geochemical studies (Gan et al., 2010; Niu, 2013), for more detail refer to Zang et al. (2020). Then these two materials were placed in an agate mortar and ground for >3 h separately, ensuring the particle size of their power was inner 10 μm. Before being used, these prepared powers were stored in a 110°C drying oven for more than 48 h to remove adsorbed water.

Experimental Procedure

The sample assemblage consisted of NaCl sleeve, Pyrex Glass, graphite furnace (with a cap), magnesium oxide (after 1,000°C heating), and the sample capsules. The power of the starting

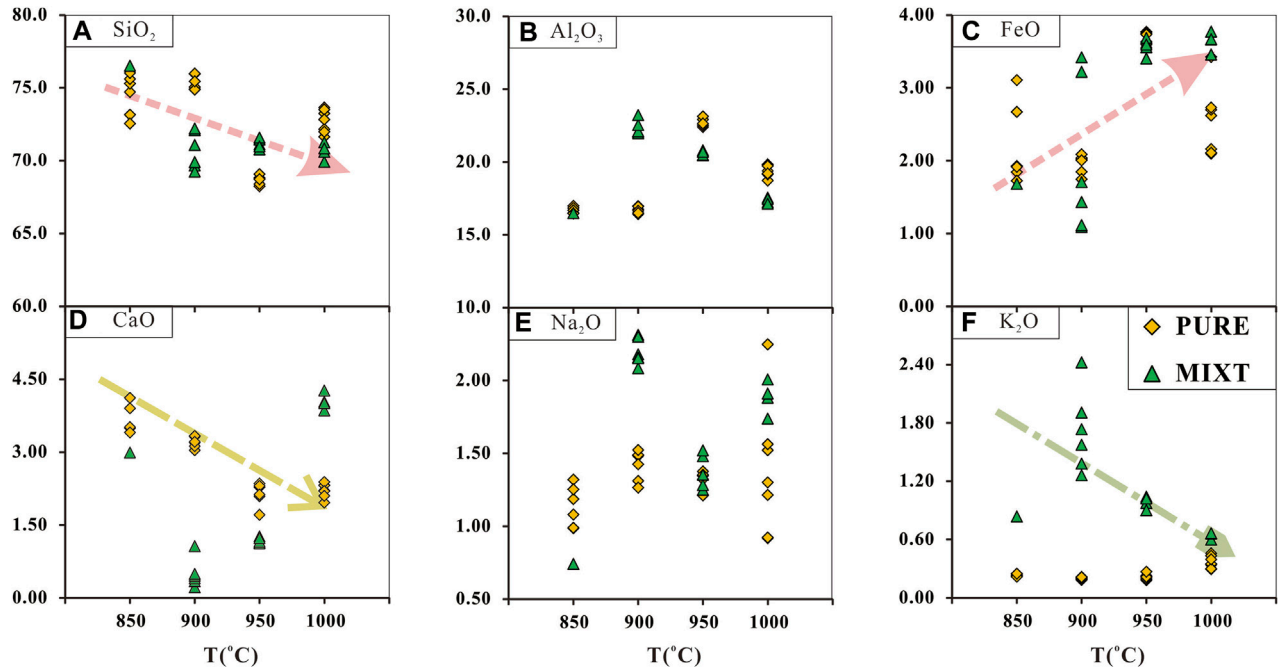

FIGURE 4 | Plots of major elements abundance of partial melts. PURE, melts generated from pure 18TH-02 (garnet plagioamphibolite, as the representative of metamorphic subducted oceanic crust); MIXT, melts generated from a mixture of 90 wt% 18TH-02 power and 10 wt% 18TH-07 (plagioclase slate, as the representative of metamorphic subducted terrigenous sediments). All the qualified original data of partial melts are shown in this figure; these data are listed in **Supplementary Table S4** original major data. The pink arrows mark the variation trend of oxide abundance in partial melts from both these two starting materials as the temperature rose. The golden yellow arrow marks the variation trend of CaO in partial melts from PURE as the temperature rose. The grass green arrow marks the variation trend of K_2O in partial melts from MITX as the temperature rose.

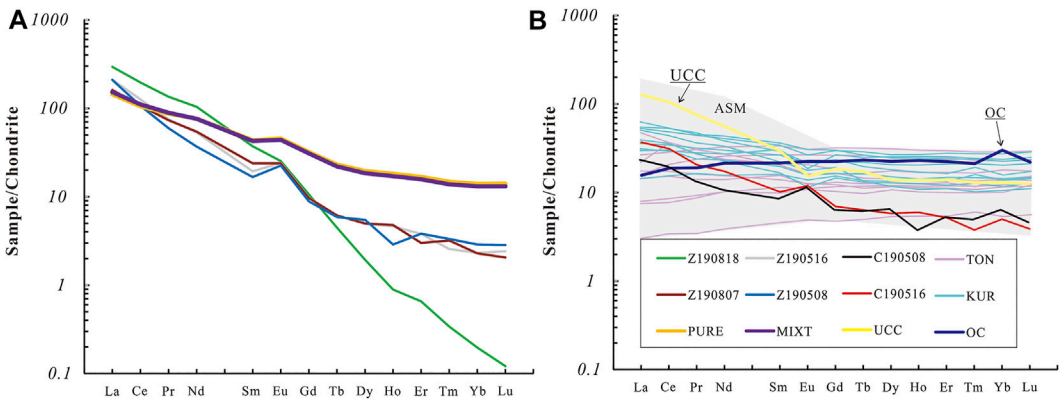

FIGURE 5 | Chondrite-normalized rare earth element (REE) abundance patterns of the partial melts **(A)** and calculated results compared with field observations **(B)**. C1-Chondrite data are from Sun and Mcdonough (1989). Z190818, Z190516, Z190708, and Z190508, partial melts from our experiment; PURE and MIXT, our starting materials. C190508 and C190516, calculated results based on our experiment data, the partition coefficient (D_i) between melts and starting material from our experiment in runs at 950°C could be got [D_i = (i in Melt)/(i in Starting material)], then we used this partition coefficient to calculate the i content in melts from pure OC (OC = oceanic crust) (C190508) and 10%UCC (UCC = Upper Continental Crust) + 90%OC (C190516), we use this method comparing the REE abundance from partial melting experiment and silicic arc magma located at Tonga Island and Kuril Island.; TON = typical REE abundance patterns from silicic magma located at Tonga Island, KUR = typical REE abundance patterns from silicic magma located at Kuril Island. ASM = arc silicic magma, REE abundance patterns from TON and KUR. Data of TON and KUR are also from the GEOROC website (http://georoc.mpch-mainz.gwdg.de/georoc/).

material was filled in gold sample capsules (with 3 mm outer diameter, 2.6 mm inner diameter, and 2.5 ± 0.2 mm height) and sealed, and then the capsule was covered by a thin hexagonal boron nitride sleeve and placed into the graphite heater. The centre of the capsule is 1 mm below the geometric centre of the graphite heater (close to the stainless steel) to get a stable thermal

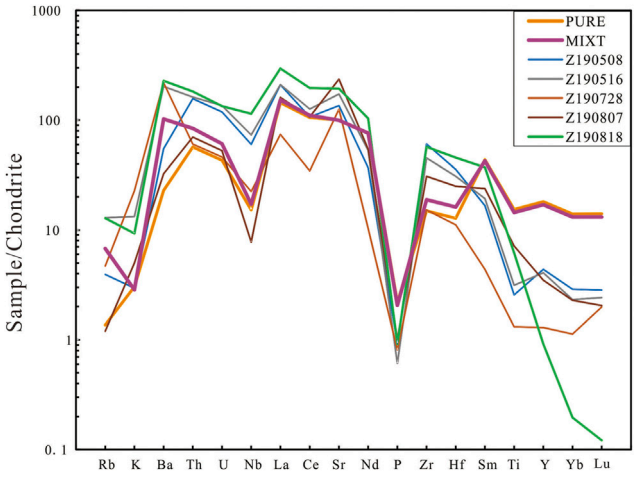

FIGURE 6 | Chondrite-normalized spidergram for the partial melts. C1-Chondrite data are from Sun and Mcdonough (1989), Z190728, Z190818, Z190516, Z190708, and Z190508, partial melts in runs from our experiment; PURE and MIXT, our starting materials.

field (Xia et al., 2014). In order to minimize adsorbed water, all the assemblies used in our experiment were heated at 110°C for 48 h before being used. Then the sample was fitted into a 10 mm diameter pressure plate one by one as shown in **Figure 2**.

All experiments were performed on a Rocktek-PC-1 type Piston-cylinder apparatus located in National Engineering Research Centre of Coal Mine Water Hazard Controlling, Suzhou University. The temperature was measured and controlled *via* NiCr-NiAl thermocouples with an accuracy of ±3°C. The temperature gradient of our sample was about 5°C, based on similar study results (Xia et al., 2014). The pressure was checked by NaCl melting (falling ball method), following the melting curve offered by Tingle et al. (1993). The error was within 0.1 GPa. According to our assessment of similar experiments, the oxygen fugacity within the experiment was close to FMQ (Tao et al., 2015), which is similar to the basaltic oceanic crust in the subducted margins.

In one run, the pressure rose to about 800 PSI by hand first. We then started heating with a 10°C/min increasing speed. When the temperature was up to 400°C, the pressure would continue to rise with a 10 PSI/min to the aim value. After the pressure rising to aim value, the temperature rose to the aim value with 10°C/min increasing speed. The pressure and temperature were maintained for 168 h, then quenched by turning the power off. The temperature fell to room temperature in 1 min. We then depressurized and removed the run product carefully from the capsule and mounted it in epoxy, which was polished for observation and analysis.

Analytical Method

The whole rock compositions (major and trace element) analyses of the two metamorphic rocks (18TH-02 and 18TH-07) were carried out in the State Key Laboratory of Ore Deposit Geochemistry, Institute of Geochemistry, Chinese Academy of Sciences, Guiyang, China. Their major elements were measured by an X-ray fluorescence spectrophotometer (XRF, PW4400, Axios), and the trace elements were measured by an inductively coupled plasma mass spectrometer (ICP-MS), in accordance with the analytical procedures given by Qi et al. (2000). Back-scattered electron (BSE) images and the major element content of minerals in these two metamorphic rocks and in the experimental products were obtained using a JOEL JXA-8100 electron microprobe at the Key Laboratory of Mineralization and Dynamics, Chang'an University, Xi'an, China. The beam used for the analyses of the melt was 5–10 μm, with an accelerating voltage of 15 kV and beam current of 2 nA. The possible losses of Na and K in the melt were addressed using the same method in Zang et al. (2020) Trace-element concentrations within the melts (glass) of run products were measured by laser ablation ICP–MS using a GeoLasPro laser ablation system and an Agilent 7700x ICP–MS instrument at the Sample Solution Analytical Technology Company, Wuhan, China. The analytical procedures used are outlined in detail by Liu et al. (2008).

EXPERIMENTAL RESULTS

Phase Assemblages

The run conditions and mineral assemblages in their products are listed in **Supplementary Table S2**. Representative BSE photographs of the experimental products are shown in **Figure 3**. There is no difference between the mineral assemblages of these two starting materials at all run conditions. In runs at 850–950°C, there are Amp + Cpx + Pl + Grt + Melt in all run products. While in runs at 1,000°C, the Amp disappeared and the mineral assemblage is Cpx + Pl + Grt + Melt. However, melts (quenched to glass) in run products of PURE are very rare. The contents of them are about 2–3 vol% in runs at 850 and 900°C. This content increases to about 5 vol% in run product at 950°C and about 10 vol% in run product at 1,000°C (**Figure 3A**). The content of melts in run products of MIXT is different from those of PURE at over 900°C. In the run at 850°C, the melt in run products of MIXT is also very rare, which is consistent with the run from PURE at 850°C. In runs at 900°C, the content of melt in MIXT's run products increases to about 10 vol%. This content increases to 20 vol % at 950°C and 35 vol% at 1,000°C (**Figure 3B**). The melting trend of MITX is consistent with the result reported by Zang et al. (2020). The mixture starting materials will increase in melting percentage at over ~925°C.

The minerals in run products of PURE at 850°C are all very small; the size of all minerals (Amp, Cpx, Grt and Pl) is all about 15 μm. In run products at over 900°C, the size of mineral crystals increases with run temperature. The size of Amp increases most obviously with the run temperature increasing, it is about 40 μm in run product at 900°C and about 100 μm in run product at 950°C. The size of the other three minerals is also increased with run temperature. The size of Cpx is 20, 30, and 50 μm respectively in runs at 900°C, 950°C, and 1,000°C. The size of Pl is 20, 40, 50 μm respectively in runs at 900°C, 950°C, and 1,000°C. The size of Grt is 20, 25, and 50 μm respectively in runs at 900°C, 950°C, and 1,000°C. The minerals in run products of MIXT at 850°C is also very small. The size of all minerals is the same as those of

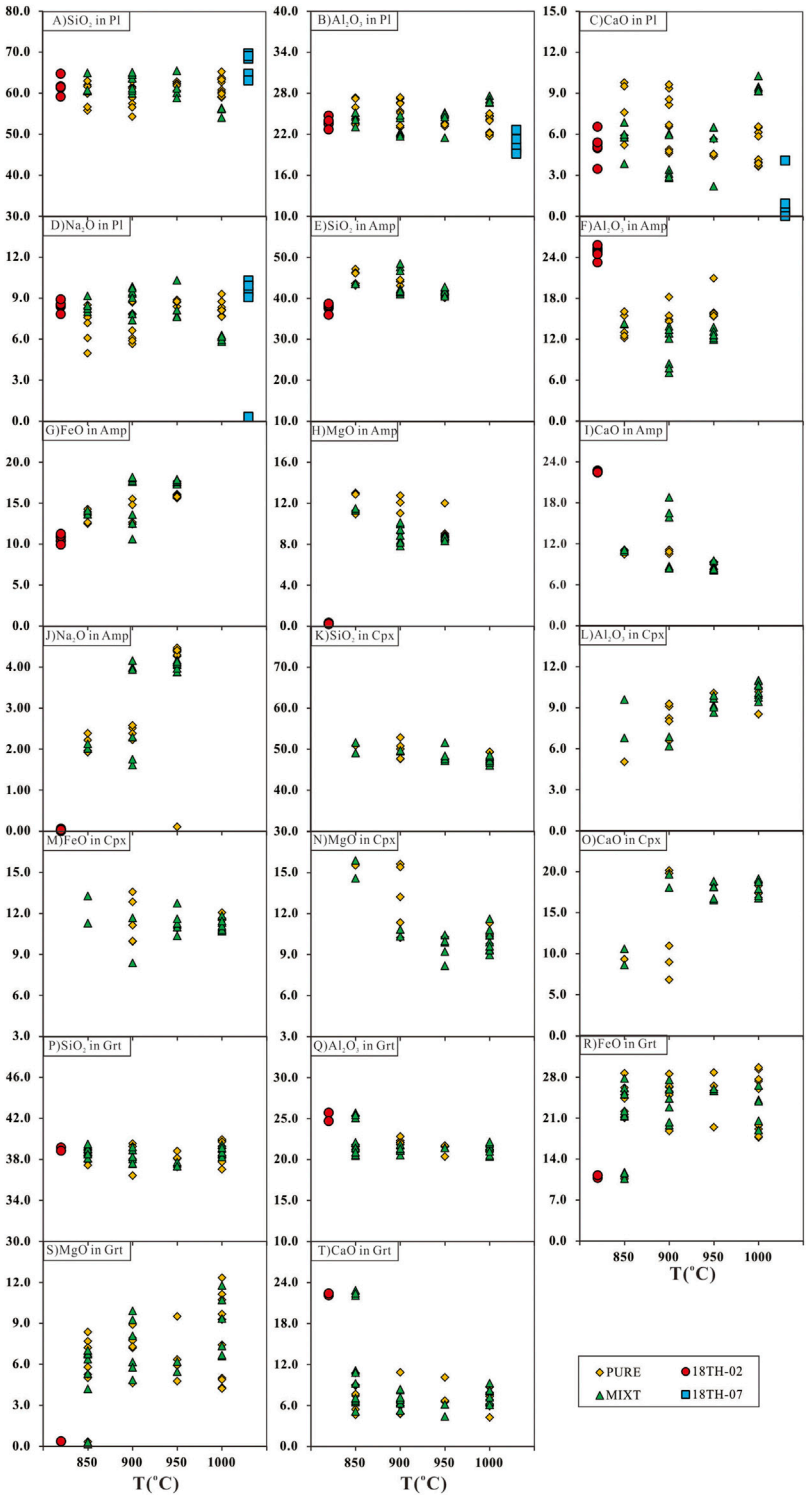

FIGURE 7 | Plots of major-element oxide concentrations in plagioclase **(A-D)**, amphibole **(E-J)**, clinopyroxene **(K-O)**, and garnet **(P-T)**. These minerals are from starting materials (18TH-02 and 18TH-07) run products from PURE and MITX.

PURE, at about 15 μm. The size of minerals in MIXT's run products is also increased with run temperature. The size of Amp is 25 and 50 μm respectively in runs at 900 and 950°C. The size of Cpx is 20, 30, and 50 μm respectively in runs of 900°C, 950°C, and 1,000°C. The size of Pl is 20, 20, and 30 μm respectively in runs at 900°C, 950°C, and 1,000°C. The size of Grt is 20, 30, and 60 μm

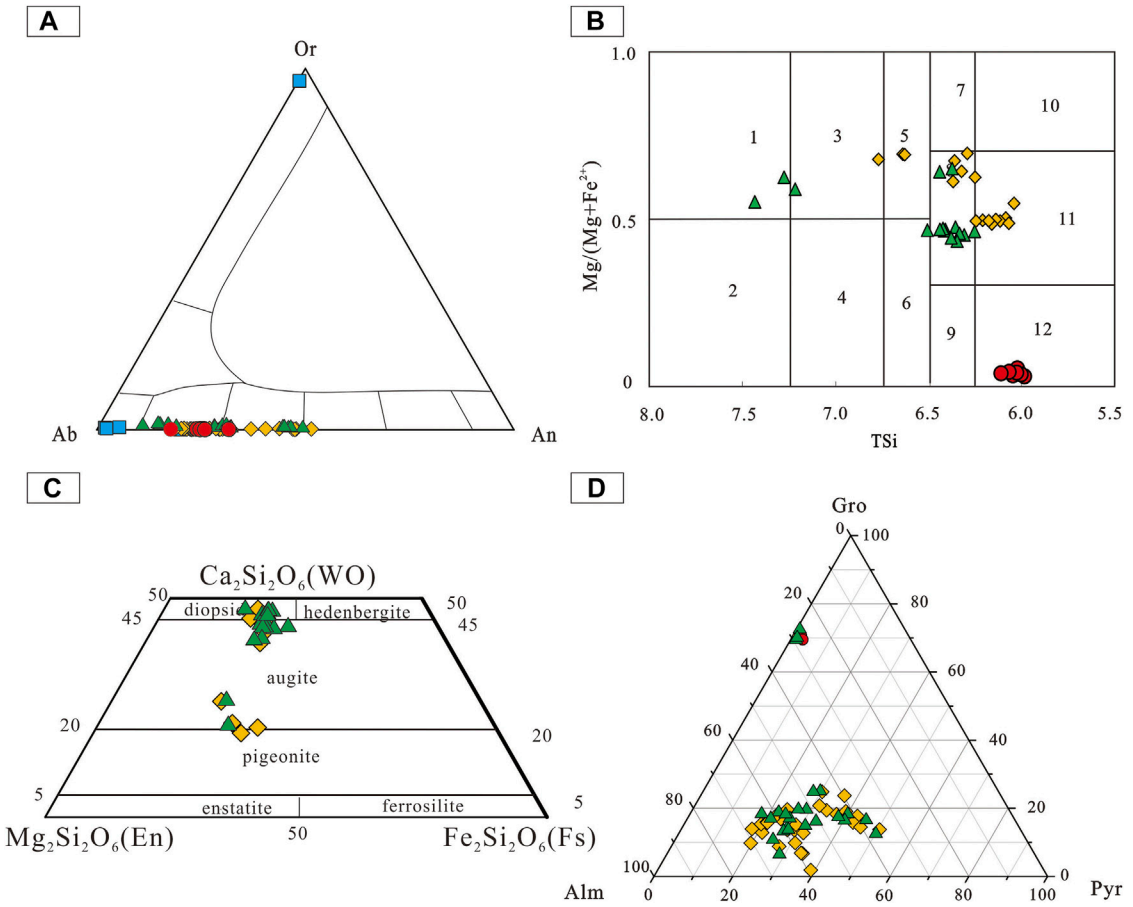

FIGURE 8 | Or-Ab-An classification map of plagioclase **(A)**, classification map of amphibole after Leake et al. (1997) **(B)**, classification map of clinopyroxene after Morimoto (1988) **(C)**, and Alm-Pyr-Gro classification map of garnet **(D)**. These minerals are mentioned in **Figure 7**.

respectively in runs at 900°C, 950°C, and 1,000°C. In all run products, Grt is euhedral crystal and other kinds of minerals are subhedral crystals.

Major Elements and Trace Element Composition of Partial Melts and Residual Minerals

The major and trace element composition of partial melts from run products reported in this paper is listed in **Supplementary Table S3**. The variation trend with run temperature rising is shown in **Figure 4**. As the run temperature rose, the SiO_2 contents of melts in all run products decreased, whereas the FeO contents of these melts show a reverse trend. The CaO content of melts from PURE showed a similar variation trend as SiO_2 contents, while the CaO content of melts from MITX at over 900°C showed a reverse trend. The K_2O content of partial melts from MIXT shows a decreasing trend as run temperature ring, while the K_2O content of partial melts from PURE is almost unchanged due to their starting materials having so little K_2O. The Al_2O_3 content of melts in all runs is between 15 and 25wt% is affected by the amount of feldspar. The Na_2O content of partial melts is about 0.5–2.5wt%. Chondrite-normalized REE patterns for the partial melts are shown in **Figure 5**. The REE patterns of the partial melts are enriched in light REE, compared with their parents, the HREE of partial melts is more depleted (**Figure 5A**). In chondrite-normalized spidergram, the partial melt depleted in Ti, Y, Yb, and Lu compared with starting material, as shown in **Figure 6**.

The SiO_2, Al_2O_3, CaO, and Na_2O content of Pl in the starting material and run products are shown in **Figure 7A–D**. Compared with the Pl in the starting material, the Pl in run products from PURE enriched in CaO and depleted in Na_2O, which was the same as the Pl in the run product at 1,000°C from MIXT. The other Pl in run products from MIXT have the same variation range with their starting material. On the Or-Ab-An classification map, all Pl in run products are plagioclase series (**Figure 8A**). The SiO_2, Al_2O_3, FeO, MgO, CaO, and Na_2O content of Amp in starting material and run products are shown in **Figure 7E–J**. Compared with starting Amp in 18TH-02, Amp in all run products is enriched in SiO_2, FeO, MgO, and Na_2O, and depleted in Al_2O_3 and CaO. This difference is also very obvious in the classification map of amphibole (Leake et al., 1997) as shown in **Figure 8B**. The SiO_2, Al_2O_3, FeO, MgO, and

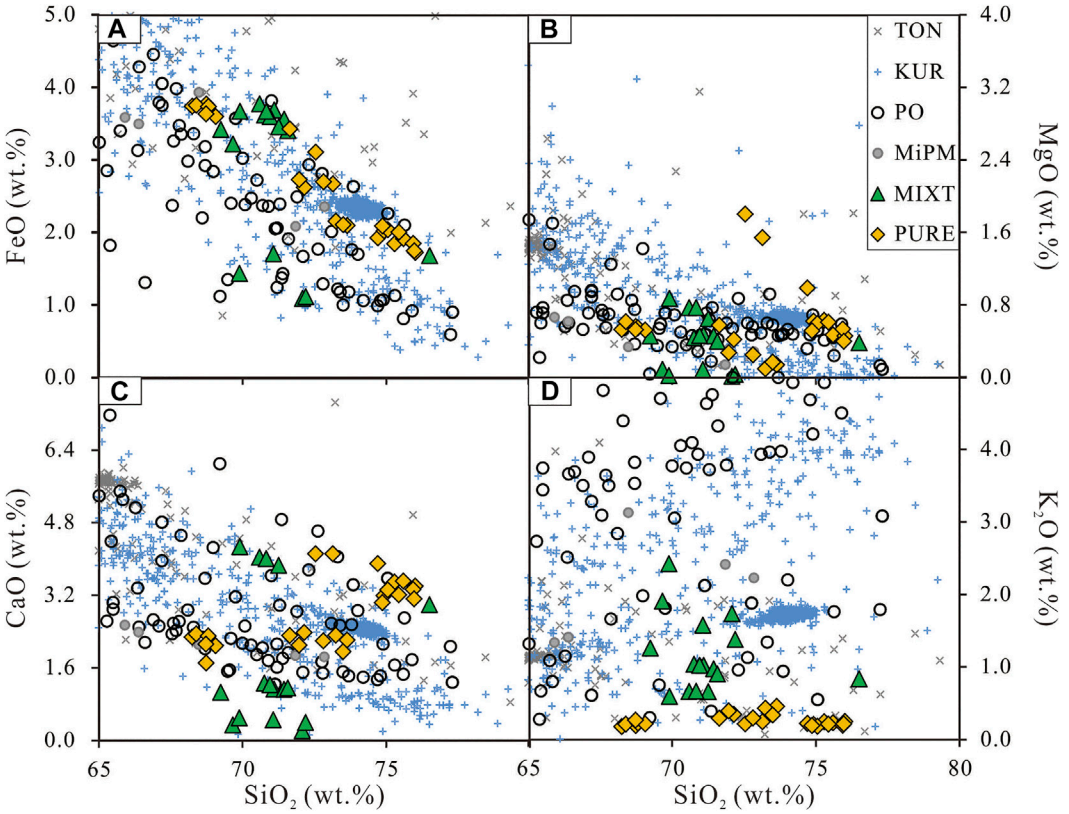

FIGURE 9 | Harker diagrams of melts from partial melting experiment and filed observation. TON, KUR, and MiPM are the same with **Figure 1** on their meaning and data; PO, melts from partial melting experiments of pure basic rocks, the data including BaDE, AmPM, and GaPM in **Figure 1**; PURE and MITX are same to **Figure 4**.

CaO content of Cpx in run products are shown in **Figure 7K–O**. As the run temperature rises, the Al_2O_3 content of Cpx in all run products increases, while the MgO content shows a reverse trend. In the classification map of clinopyroxene (Morimoto, 1988), the Cpx from runs at 850 and 900°C are enriched in En and others enriched in Wo (**Figure 8C**). The SiO_2, Al_2O_3, FeO, MgO, and CaO content of Grt in starting material and run products are shown in **Figure 7P–T**. Compared with the starting Grt in 18TH-02, the Grt in all run products was enriched in FeO and MgO, and depleted in CaO, which is consistent with the Alm-Pyr-Gro classification map, as shown in **Figure 8D**.

DISCUSSION

Firstly, we need to consider whether the equilibrium was approached in our run products. According to similar experimental studies (Beard and Lofgren, 1991; Sen and Dunn, 1994; Xiong et al., 2005; Qian and Hermann, 2013; Zang et al., 2020) that undertook partial experiments at ≥900°C, a run time of ≥96 h could be regarded as approaching equilibrium. Our run time was 168 h, nearly twice as long as the run time used in previous studies to approach equilibrium, meaning the melts (glass) in our run products show component differences (**Figure 4**). The component difference of melt may be caused by poor liquidity due to low degree partial melting. The equilibrium in our run products should be a local one. Furthermore, the Fe–Mg exchange distribution coefficients ($K_{d,\ Fe-Mg}$) of mineral–melt were also calculated. The $K_{d,\ Fe-Mg}$ value of Cpx was 0.06–0.53, the $K_{d,\ Fe-Mg}$ value of Grt was 0.32–1.71, compared with the value of similar studies (Xiong et al., 2005; Qian and Hermann, 2013; Zang et al., 2020). These $K_{d,\ Fe-Mg}$ values of minerals are acceptable, indicating the equilibrium is approached. The major and trace element compositions at different sites are homogeneous (within analytical error), indicating that equilibrium was attained.

Comparison Between Melts From PURE and MITX

We then compared melts from PURE and MITX. With the sediment addition, the MITX increased its melting percentage at over 900°C, which is the same as previous studies (Mccarthy and Patiño Douce, 1997; Zang et al., 2020), but the melting percentage in this study is very small compared with others. The reasons for this may be the following: 1) there is no free water added in our experiment: the water in our run products is from dehydration of Amp in staring materials (18 TH-02). The water content of our experiment is lower than similar experiments with water added before the Amp is destroyed. 2) These two staring

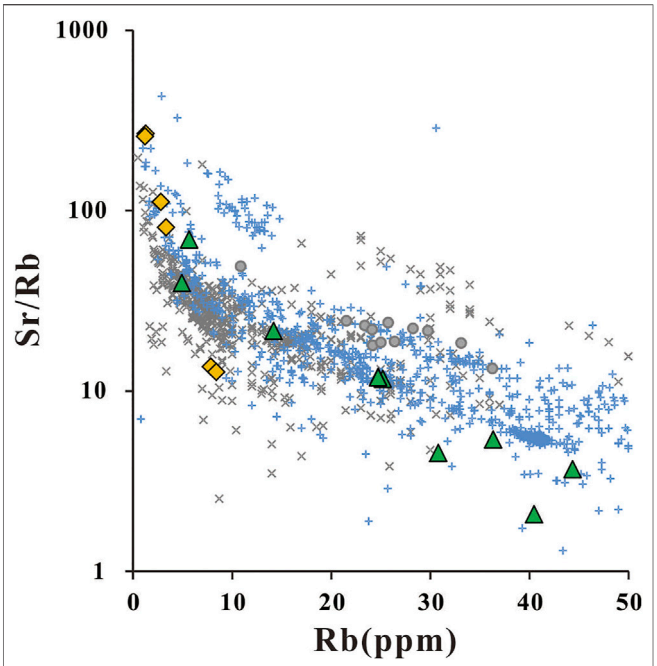

FIGURE 10 | Plots of Sr/Rb VS Rb. Symbols are the same as **Figure 9**, the original data of PURE and MITX are listed in **Supplementary Table S5** original trace data. Then we used the same computing method mentioned in **Figure 5** to revise our data. The trace element data of melts from pure basic rocks (Xiong et al., 2006; Qian and Hermann, 2013) are out of the variation range, so there are no OP data shown in this figure.

materials are metamorphic rocks, unlike basalt, there is no glass in them. By comparing the melting percentage of PURE and MITX, the melt percentage of MIXT is much higher than the one of PURE in runs at 950and 1,000°C, and the increasing value of MITX is more than the total content of addition metamorphic subducted terrigenous sediment. This result indicates the effect of sediment addition on increasing melting percentage needs a "staring temperature" (950°C in this paper). The addition sediments significantly help the partial melting of subducted oceanic crust over this staring temperature.

We then compared the chemical composition of melt from PURE and MIXT over the staring temperature, to consider which one could be the real magma. As shown in **Figure 4** the melt from MIXT are enriched in Na_2O and K_2O and depleted in Al_2O_3 in major elements than the melt from PURE in runs at 950and 1,000°C. For trace elements, the melts from the mixture enrich more in Rb than the PURE because the MIXT has a very high content of Rb compared to PURE.

Affect of Sediment Addition on Silicic Arc Magma Generation

Possible ways in which the silicic arc magma is generated include: 1) that it is generated by partial melting of the subducted altered oceanic crust; or 2) that it could have evolved from mantle-derived mafic magmas (see Clemens et al. (2021) and references therein). It seems unlikely that the majority of silicic melt could be evolved from basalt for the following reasons: 1) silicic melt has a high viscosity and crystallization differentiation is difficult (even this process could be achieved with a large number of chadacrysts that are not completely separated from silicic magma, but the chadacrysts are not so widely distributed); 2) the crystallization differentiation of magma could be detected *via* geochemical data, such as separation of feldspar can lead to Eu anomalies, however, there are no obvious Eu anomalies in current data relating to rocks ($SiO2 \geq 52$wt%) from Tonga and Kuril (**Figure 5B**). The partial of subducted altered oceanic crust with or without sediments could be an important way of generating silicic magma at convergent plate margins.

In terms of the effect of sediment addition on silicic arc magma generation, we compared the major element content of rocks from field observation and melt from partial experiments on basic rocks and basalt-sediment mixtures *via* Harker diagrams (**Figure 9**). For major elements, melts from the experiment seem to all cover the variation range of arc silicic magma located on Tonga and the Kuril Islands. The melts from MIXT also match the field observation better on the SiO_2-K_2O diagram because the PURE (and the oceanic crust) is depleted on K_2O. The high K_2O silicic magmas may thus generate from the mixture of magmatic sources. Besides the major elements, the trace element of rocks from field observation and melt from partial experiments are also compared *via* plots of Sr/Rb—Rb (**Figure 10**). Unlike the major elements, the melts from the mixture match the field observation better. Note that the trace element data on melts from pure basic rocks (Xiong et al., 2006; Qian and Hermann, 2013) are out of the variation range shown in **Figure 10**. Furthermore, the REE abundance patterns of partial melts from magmatic sources with sediment addition have an obvious right-leaning than the one from the pure magmatic source. The partial melts from the mixture magmatic sources match the silicic magma from Kuril Island better than the melts from pure magmatic sources. This result indicates that the arc silicic magma is mainly generated from the partial melting of a mixture of basic oceanic crust and sediments. The sediments also offer great help in establishing the partial melting percentage. This may also contribute to the formation of silicic arc magma.

CONCLUSION

Our experiments reveal that the addition of 10 wt% sediment has an obvious effect on the partial melting of basic rocks. These results are based on examination of the chemical composition of experimental partial melts produced from a series of comparative partial melting experiments on a garnet plagioamphibolite and a 90 wt% garnet plagioamphibolite +10 wt% plagioclase slate mixture at 850–1,000°C/1.5 GPa. The importance of sediment addition was also verified and identified in the generation of arc silicic magma. The main conclusions of this study are as follows:

1) A small additional amount of (10 wt%) altered sediment makes the metamorphic subducted oceanic crust generate

more silicic melt with geochemical characteristics of higher Na_2O and K_2O and lower Al_2O_3 in major element and high Rb content in trace element at over 950°C.

2) Silicic arc magma may generate from partial melting of metamorphic subducted oceanic crust with sediments thereon. The addition of sediment contributes to their high Rb content and the partial melting percentage of their parent rock.

DATA AVAILABILITY STATEMENT

The original contributions presented in the study are included in the article/**Supplementary Material**, further inquiries can be directed to the corresponding author.

AUTHOR CONTRIBUTIONS

All authors listed have made a substantial, direct, and intellectual contribution to the work and approved it for publication.

FUNDING

This work was financially supported by the Natural Science Foundation of China (No. 42073059 and No. 41502057), the Youth Project of the Provincial Natural Science Foundation of Anhui (2108085QD162), and the Foundation of Suzhou University (No. gxyq2020060, No. 2019XJZY53).

ACKNOWLEDGMENTS

We are grateful to the two reviewers for their helpful comments and suggestions on the manuscript. We thank Lidong Dai for his invitation, Minwu Liu for support and help in electron microprobe analysis.

SUPPLEMENTARY MATERIAL

The Supplementary Material for this article can be found online at: https://www.frontiersin.org/articles/10.3389/feart.2022.851236/full#supplementary-material

REFERENCES

Baker, M. B., Hischmann, M. M., Ghiorso, M. S., and Stolper, E. M. (1995). Compositions of Near-Solidus Peridotite Melts from Experiments and Thermodynamic Calculations. *Nature* 375, 308–311. doi:10.1038/375308a0

Beard, J. S., and Lofgren, G. E. (1991). Dehydration Melting and Water-Saturated Melting of Basaltic and Andesitic Greenstones and Amphibolites at 1, 3, and 6. 9 Kb. *J. Petrol.* 32, 465–501. doi:10.1093/petrology/32.2.365

Clemens, J. D., Stevens, G., and Mayne, M. J. (2021). Do arc Silicic Magmas Form by Fluid-Fluxed Melting of Older Arc Crust or Fractionation of Basaltic Magmas? *Contrib. Mineral. Petrol.* 176, 44. doi:10.1007/s00410-021-01800-w

Cruz-Uribe, A. M., Marschall, H. R., Gaetani, G. A., and Le Roux, V. (2018). Generation of Alkaline Magmas in Subduction Zones by Partial Melting of Mélange Diapirs-An Experimental Study. *Geology* 46, 343–346. doi:10.1130/g39956.1

Elliott, T. (2003). Tracers of the Slab. *Geophys. Monogr. Ser.* 238, 23–45. doi:10.1029/138gm03

Frster, M. W., and Selway, K. (2021). Melting of Subducted Sediments Reconciles Geophysical Images of Subduction Zones. *Nat. Commun.* 12, 1320. doi:10.1038/s41467-021-21657-8

Gan, L., Tang, H., and Han, Y. (2010). Geochronology and Geochemical Characteristics of Yemaquan Granitic Pluton in East Junggar, Xinjiang. *Act a petrologica sinica* 26, 2374–2388. (in Chinese with English abstract).

Hermann, J., and Spandler, C. J. (2008). Sediment Melts at Sub-arc Depths: an Experimental Study. *J. Petrol.* 49, 717–740. doi:10.1093/petrology/egm073

Hildreth, W., and Moorbath, S. (1988). Crustal Contributions to Arc Magmatism in the Andes of Central Chile. *Contr. Mineral. Petrol.* 98, 455–489. doi:10.1007/bf00372365

Hu, Y., Teng, F. Z., Plank, T. A., and Huang, K. J. (2017). Magnesium Isotopic Composition of Subducting Marine Sediments. *Chem. Geology.* 46, 15–31. doi:10.1016/j.chemgeo.2017.06.010

Koepke, J. r., Feig, S. T., Snow, J., and Freise, M. (2004). Petrogenesis of Oceanic Plagiogranites by Partial Melting of Gabbros: an Experimental Study. *Contrib. Mineralogy Petrol.* 146, 414–432. doi:10.1007/s00410-003-0511-9

Leake, B. E., Woolley, A. R., Arps, C. E. S., Birch, W. D., Gilbert, M. C., Grice, J. D., et al. (1997). Nomenclature of Amphiboles; Report of the Subcommittee on Amphiboles of the International Mineralogical Association Commission on New Minerals and Mineral Names. *Mineral. Mag.* 61, 295–310. doi:10.1180/minmag.1997.061.405.13

Li, W., and Ni, H. (2020). Dehydration at Subduction Zones and the Geochemistry of Slab Fluids. *Sci. China Earth Sci.* 63, 1925–1937. doi:10.1007/s11430-019-9655-1

Liu, Y., Chen, C., He, D., and Chen, W. (2019). Deep Carbon Cycle in Subduction Zones. *Sci. China Earth Sci.* 62, 1764–1782. doi:10.1007/s11430-018-9426-1

Liu, Y., Hu, Z., Gao, S., Günther, D., Xu, J., Gao, C., et al. (2008). In Situ Analysis of Major and Trace Elements of Anhydrous Minerals by LA-ICP-MS Without Applying an Internal Standard. *Chem. Geol.* 257, 34–43.

Maitre, R. W. L. (1989). *A Classification of Igneous Rocks and Glossary of Terms : Recommendations of the International Union of Geological Sciences Subcommission on the Systematics of Igneous Rocks* Blackwell.

Mccarthy, T. C., and Patiño Douce, A. E. (1997). Experimental Evidence for High-Temperature Felsic Melts Formed during Basaltic Intrusion of the Deep Crust. *Geol* 25, 463–466. doi:10.1130/0091-7613(1997)025<0463:eefhtf>2.3.co;2

Morimoto, N. (1988). Nomenclature of Pyroxenes. *Mineralogy Petrol.* 39, 55–76. doi:10.1007/bf01226262

Morris, J. D., Leeman, W. P., and Tera, F. (1990). The Subducted Component in Island Arc Lavas: Constraints from Be Isotopes and B-Be Systematics. *Nature* 344, 31–36. doi:10.1038/344031a0

Nandedkar, R. H., Ulmer, P., and Müntener, O. (2014). Fractional Crystallization of Primitive, Hydrous Arc Magmas: an Experimental Study at 0.7 GPa. *Contrib. Mineral. Petrol.* 167, 1015. doi:10.1007/s00410-014-1015-5

Nielsen, S. G., and Marschall, H. R. (2017). Geochemical Evidence for Mélange Melting in Global Arcs. *Sci. Adv.* 3, e1602402. doi:10.1126/sciadv.1602402

Niu, Y. (2013). *Global Tectonics and Geodynamics : A Petrological and Geochemical Approach*. Beijing: science press.

Pelleter, A. A., Prouteau, G., and Scaillet, B. (2021). The Role of sulphur on the Melting of Ca-Poor Sediment and on Trace Element Transfer in Subduction Zones: an Experimental Investigation. *J. Petrol.* 62, egab005. doi:10.1093/petrology/egab005

Peter, U., Ralf, K., and Othmar, M. (2018). Experimentally Derived Intermediate to Silica-Rich Arc Magmas by Fractional and Equilibrium Crystallization at 1·0 GPa: an Evaluation of Phase Relationships, Compositions, Liquid Lines of Descent and Oxygen Fugacity. *J. Petrol.* 59, 11–58. doi:10.1093/petrology/egy017

Plank, T. (2005). Constraints from Thorium/Lanthanum on Sediment Recycling at Subduction Zones and the Evolution of the Continents. *J. Petrol.* 46, 921–944. doi:10.1093/petrology/egi005

Qi, L., Jing, H., and Gregoire, D. C. (2000). Determination of Trace Elements in Granites by Inductively Coupled Plasma Mass Spectrometry. *Talanta* 51, 507–513. doi:10.1016/s0039-9140(99)00318-5

Qian, Q., and Hermann, J. (2013). Partial Melting of Lower Crust at 10-15 Kbar: Constraints on Adakite and TTG Formation. *Contrib. Mineral. Petrol.* 165, 1195–1224. doi:10.1007/s00410-013-0854-9

Rapp, R. P., and Watson, E. B. (1995). Dehydration Melting of Metabasalt at 8-32 Kbar: Implications for Continental Growth and Crust-Mantle Recycling. *J. Petrol.* 36, 891–931. doi:10.1093/petrology/36.4.891

Rapp, R. P., Watson, E. B., and Miller, C. F. (1991). Partial Melting of Amphibolite/eclogite and the Origin of Archean Trondhjemites and Tonalites. *Precambrian Res.* 51, 1–25. doi:10.1016/0301-9268(91)90092-o

Rushmer, T. (1991). Partial Melting of Two Amphibolites: Contrasting Experimental Results under Fluid-Absent Conditions. *Contr. Mineral. Petrol.* 107, 41–59. doi:10.1007/bf00311184

Sen, C., and Dunn, T. (1994). Dehydration Melting of a Basaltic Composition Amphibolite at 1.5 and 2.0 GPa: Implications for the Origin of Adakites. *Contr. Mineral. Petrol.* 117, 394–409. doi:10.1007/bf00307273

Shu, Y., Nielsen, S. G., Zeng, Z., Shinjo, R., and Shuai, C. (2017). Tracing Subducted Sediment Inputs to the Ryukyu Arc-Okinawa Trough System: Evidence from Thallium Isotopes. *Geochimica Et Cosmochimica Acta* 217, 462–491. doi:10.1016/j.gca.2017.08.035

Sisson, T. W., Ratajeski, K., Hankins, W. B., and Glazner, A. F. (2005). Voluminous Granitic Magmas from Common Basaltic Sources. *Contrib. Mineral. Petrol.* 148, 635–661. doi:10.1007/s00410-004-0632-9

Sun, S. S., and Mcdonough, W. F. (1989). Chemical and Isotopic Systematics of Oceanic Basalts: Implications for Mantle Composition and Processes. *Geol. Soc. Spec. Publ.* 42, 313–345.

Sun, W., Teng, F.-Z., Niu, Y.-L., Tatsumi, Y., Yang, X.-Y., and Ling, M.-X. (2014). The Subduction Factory: Geochemical Perspectives. *Geochimica Et Cosmochimica Acta* 143, 1–7. doi:10.1016/j.gca.2014.06.029

Takahahshi, E., Nakajima, K., and Wright, T. L. (1998). Origin of the Columbia River Basalts: Melting Model of a Heterogeneous Plume Head. *Earth Planet. Sci. Lett.* 162, 63–80. doi:10.1016/s0012-821x(98)00157-5

Tao, R., Zhang, L., and Liu, X. (2015). Oxygen Fugacity of Earth's Mantle and Deep Carbon Cycle in the Subduction Zone. *Acta Petrologica Sinica* 31, 1879–1890.

Tatsumi, Y. (2001). Geochemical Modeling of Partial Melting of Subducting Sediments and Subsequent Melt-Mantle Interaction: Generation of High-Mg Andesites in the Setouchi Volcanic belt, Southwest Japan. *Geol* 29, 323–326. doi:10.1130/0091-7613(2001)029<0323:gmopmo>2.0.co;2

Tera, F., Brown, L., Morris, J., Sacks, I. S., Klein, J., and Middleton, R. (1986). Sediment Incorporation in Island-Arc Magmas: Inferences from 10Be. *Geochimica Et Cosmochimica Acta* 50, 535–550. doi:10.1016/0016-7037(86)90103-1

Tingle, T. N., Green, H. W., Young, T. E., and Koczynski, T. A. (1993). Improvements to Griggs-type Apparatus for Mechanical Testing at High Pressures and Temperatures. *Pageoph* 141, 523–543. doi:10.1007/bf00998344

Wang, X. C., Wilde, Z. A., Li, C., Lei, S. K., and Pandit, K. (2021). Decoupling between Oxygen and Radiogenic Isotopes − Evidence for Generation of Juvenile continental Crust by Partial Melting of Subducted Oceanic Crust. *J. Earth Sci.* 32, 14. doi:10.1007/s12583-020-1095-2

Wei, C., and Zheng, Y. (2020). Metamorphism, Fluid Behavior and Magmatism in Oceanic Subduction Zones. *Sci. China Earth Sci.* 63, 52–77. doi:10.1007/s11430-019-9482-y

Xia, Y., Xing, D., Song, M., Xiong, X., and Hao, X. (2014). Temperature Determination and Thermal Structure Analysis on the Pressure Assembly of a Piston-Cylinder Apparatus. *Chin. J. High Press. Phys.* 28, 262–272. doi:10.11858/gywlxb.2014.03.002

Xiong, X., Adam, J., Green, T. H., Niu, H., Wu, J., and Cai, Z. (2006). Trace Element Characteristics of Partial Melts Produced by Melting of Metabasalts at High Pressures: Constraints on the Formation Condition of Adakitic Melts. *Sci. China Ser. D* 49, 915–925. doi:10.1007/s11430-006-0915-2

Xiong, X. L., Adam, J., and Green, T. H. (2005). Rutile Stability and Rutile/melt HFSE Partitioning during Partial Melting of Hydrous basalt: Implications for TTG Genesis. *Chem. Geology.* 218, 339–359. doi:10.1016/j.chemgeo.2005.01.014

Xiong, X., Xingcheng, L., Li, L., Jintuan, W., Wei, C., Mengfei, R., et al. (2020). The Partitioning Behavior of Trace Elements in Subduction Zones: Advances and Prospects. *Sci. China Earth Sci.* 63, 1938–1951. doi:10.1007/s11430-019-9631-6

Yaxley, G. M., and Green, D. H. (1998). Reactions between Eclogite and Peridotite: Mantle Refertilisation by Subduction of Oceanic Crust. *Schweizerische Mineralogische Und Petrographische Mitteilungen* 78, 243–255.

Zang, C., Tang, H., and Wang, M. (2020). Effects of Sediment Addition on Magma Generation from Oceanic Crust in a post-collisional Extensional Setting: Constraints from Partial Melting Experiments on Mudstone-Amphibolite/basalt at 1.0 and 1.5 GPa. *J. Asian Earth Sci.* 188, 104111. doi:10.1016/j.jseaes.2019.104111

Zhang, Y., Liang, X., Wang, C., Jin, Z., Zhu, L., and Gan, W. (2020). Experimental Constraints on the Partial Melting of Sediment-Metasomatized Lithospheric Mantle in Subduction Zones. *Am. Mineral.* 105, 1191–1203. doi:10.2138/am-2020-7403

Zhang, Y., Wang, C., Zhu, L., Jin, Z., and Li, W. (2019). Partial Melting of Mixed Sediment-Peridotite Mantle Source and its Implications. *J. Geophys. Res. Solid Earth* 124, 6490–6503. doi:10.1029/2019jb017470

Zhang, Z., Ding, H., Dong, X., and Tian, Z. (2020). Partial Melting of Subduction Zone. *Act a petrologica sinica* 36, 27. doi:10.18654/1000-0569/2020.09.01

Zheng, J., Xiong, Q., Zhao, Y., and Li, W. (2019). Subduction-zone Peridotites and Their Records of Crust-Mantle Interaction. *Sci. China Earth Sci.* 62, 1033–1052. doi:10.1007/s11430-018-9346-6

Zheng, Y., Chen, Y., Dai, L., and Zhao, Z. (2015). Developing Plate Tectonics Theory from Oceanic Subduction Zones to Collisional Orogens. *Sci. China Earth Sci.* 58, 1045–1069. doi:10.1007/s11430-015-5097-3

Conflict of Interest: The authors declare that the research was conducted in the absence of any commercial or financial relationships that could be construed as a potential conflict of interest.

Publisher's Note: All claims expressed in this article are solely those of the authors and do not necessarily represent those of their affiliated organizations, or those of the publisher, the editors and the reviewers. Any product that may be evaluated in this article, or claim that may be made by its manufacturer, is not guaranteed or endorsed by the publisher.